Electronic Supplementary Material (ESI) for Soft Matter.

Supplementary Information

PBTTT-C_{16} sol-gel transition by hierarchical colloidal bridging

Han-Liou Yi and Chi-Chung Hua*

Department of Chemical Engineering, National Chung Cheng University, Chiayi 62102, Taiwan

S1 Comparison of pBTTT-C_{14} and pBTTT-C_{16} solutions under varying experimental conditions

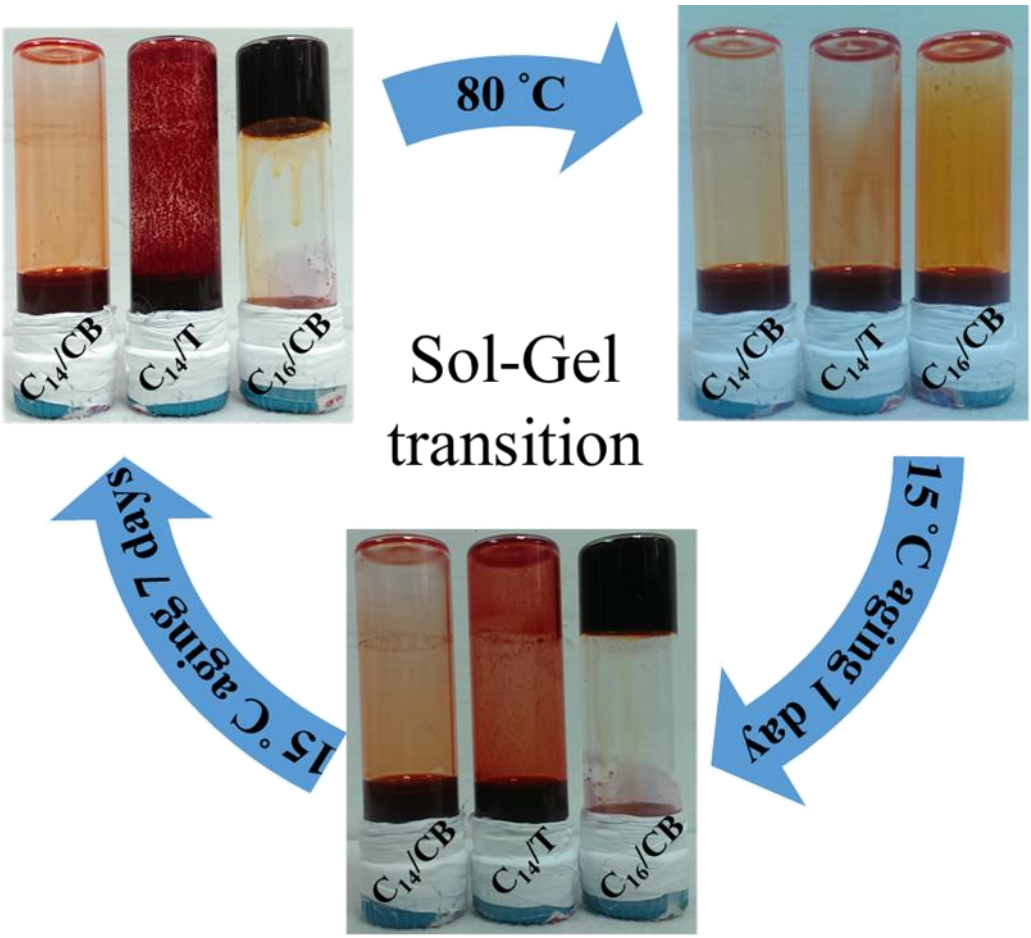

Fig. S1 Photographs showing the outer apperances of freshly prepared 10 mg/mL pBTTT solutions (pBTTT-C_{14}/CB, pBTTT-C_{14}/T, and Hw-pBTTT-C_{16}/CB) at 80 °C (upper right) and after 1 (bottom) or 7-day (upper left) aging at 15 °C.

S2 Absorbance of Hw-pBTTT-C_{16}/CB solution and gels

A UV-vis spectrometer (JASCO, V-570) was employed to examine the absorbance of Hw-pBTTT-C_{16}/CB solution and gels. The measurement was conducted with a cell having a path length of 2 mm (Hellma, 110-QS) to minimize the scattering associated with large Hw-pBTTT-C_{16} clusters. **Fig. S2** reveals that the present Hw-pBTTT-C_{16}/CB samples have negligible absorption at the incident light wavelength (λ_0 = 785 nm) used in this work.

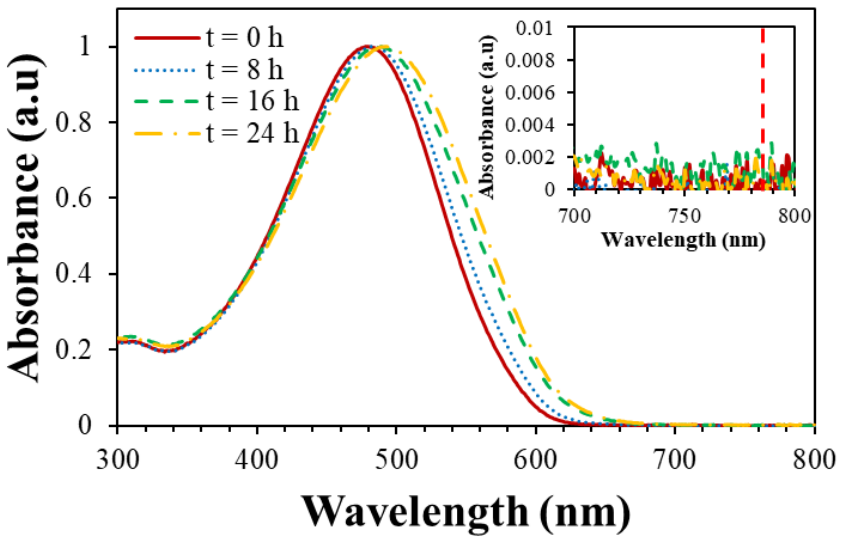

Fig. S2 Time evolutions of the UV-vis absorption spectra during the Hw-pBTTT-C_{16}/CB sol-gel transition at T = 15 °C, where results at four different gelation times are shown: t = 0 h (solid line), 8 h (dotted line), 16 h (dashed line), and 24 h (dashed-dotted line). The absorption at 785 nm is marked by the vertical dashed line in the magnified inset figure.

S3 Effect of laser power on the dynamics of Hw-pBTTT-C$_{16}$/CB gel

Fig. S3 shows the effect of incident laser power on the intensity correlation function, $g^{(2)}(q,t) - 1$, for a Hw-pBTTT-C$_{16}$/CB gel. It is apparent that $g^{(2)}(q,t) - 1$ obtained under 50% of the incident laser power (20 mW) differs considerably from those of 25% and 5%. According to the wavy feature at long decay times, it is possible that laser-induced convection has some effect on the the relaxation spectrum of the Hw-pBTTT-C$_{16}$/CB gel. As the incident laser power is reduced to 5% of its original intensity, however, it seems that such an effect can be minimized.

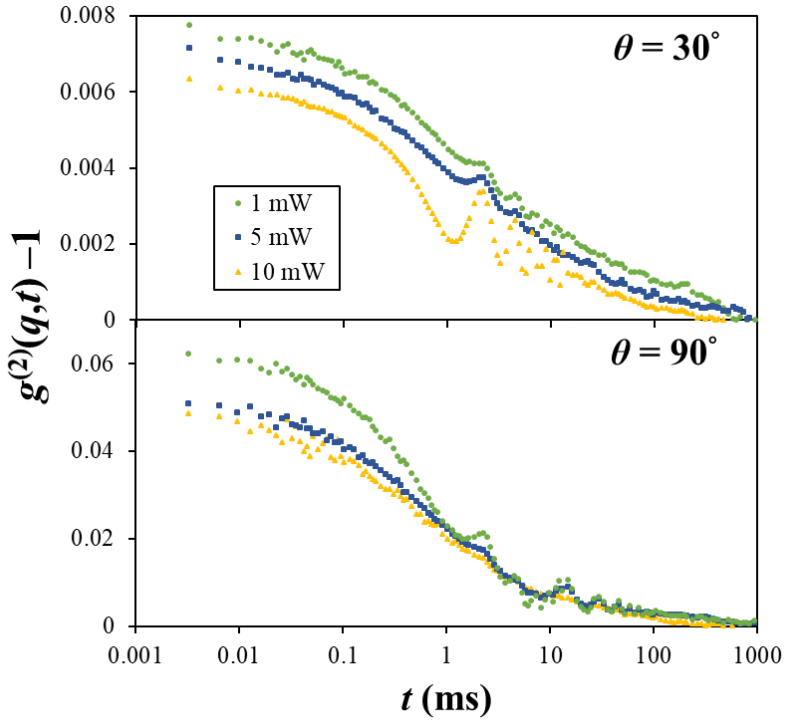

Fig. S3 Intensity correlation functions, $g^{(2)}(q,t) - 1$, for the Hw-pBTTT-C$_{16}$/CB gel incubated at T = 15 °C (t = 24 h), with the laser power equal to 5%, 10% or 50% of the original intensity. The results for two representative scattering angles are shown.

S4 Assessment of ergodicity of Hw-pBTTT-C$_{16}$/CB gels

Nonergodic media, such as glasses[1,2] and gels,[3] are known to bear frozen spatial inhomogeneities due to the effects of frozen structure (in glasses) and topological constraint, i.e., cross-linking (in gels).[4] Among the most noticeble manifestations of nonergodicity is the appearance of speckles, i.e., random fluctuations in scattering intensity with varying sample position. At early times, it was generally believed that spatial inhomogeneities are a characteristic feature of chemical gels so that speckles won't be observable in physical gels. More recently, there have been numerous examples clearly demonstrating that the previous hypothesis is incorrect, considering, for instance, PVA/CR gel,[5] gelatin gel,[6,7] and hybrid gel.[8] The notion of nonergodicity, first advocated by Pusey and Van Megen,[4] has led to the subsequent development of analysis schemes for resolving the dynamic properties of gels, including partial heterodyne method[9,10] and intermediate scattering function analysis.[11]

For nonergodic gels, the time-averaged scattering intensity $\langle I \rangle_T$ accommodates two distinct contributions denoted as $\langle I \rangle_T = \langle I_s \rangle_T + \langle I_d \rangle_T$,[12] where $\langle I_s \rangle_T$ represents the frozen-in component that changes with varying sample position, and $\langle I_d \rangle_T$ is the mobile (or intrinsic) dynamic component that is independent of the sample position. At each randomly selected position, one simultaneously measures $\langle I \rangle_T$ from static light scattering (SLS) and $g^{(2)}(q, t)$ from dynamic light scattering (DLS) at a given scattering angle.[9,10,13] According to partial heterodyne method, the contribution from the mobile dynamic component, $\langle I_d \rangle_T$, may be obtained through the following relation:[8,10,14-18]

$$\frac{\langle I \rangle_T}{D_A} = \frac{2\langle I \rangle_T}{D} - \frac{\langle I_d \rangle_T}{D} \tag{S1}$$

where D_A denotes the apparent diffusion coefficient and D is the collective diffusion coefficient in pure

heterodyne. The experimental strategy is as follows: at each randomly selected sample position, $\langle I \rangle_T$ can be obtained from the SLS experiment while D_A can be simultaneously extracted from $g^{(2)}(q, t)$ in the DLS experiment. Then, the values of D and $\langle I_d \rangle_T$ can be estimated from the slope and intercept, respectively, of the plot of $\langle I \rangle_T / D_A$ versus $\langle I \rangle_T$. On the other hand, the ensemble-averaged scattering intensity, $\langle I \rangle_E$, is evaluated by $\sum_i \langle I \rangle_{T,i} / N$, with N being the total number of randomly selected sample positions (N = 100 in this experiment). Only in an ergodic system will $\langle I \rangle_E = \langle I \rangle_T$ and $\langle I_s \rangle_T = 0$ hold true. Note that the disparity between $\langle I_d \rangle_T$ and $\langle I \rangle_E$ reflects the degree of nonergodicity.

Fig. S4 presents the time-averaged scattering intensity, $\langle I \rangle_T$, for Hw-pBTTT-C_{16}/CB solution and gel, as the sample position was arbitrarily chosen by rotating and lifting the sample cuvette. It can be seen that at T = 80 °C the speckle pattern vanishes because the solution remains as a uniform dispersion. In contrast, a notable speckle pattern emerges for the gel, and nonergodicity clearly reflects in the marked difference between $\langle I \rangle_E$ and $\langle I_d \rangle_T$. The value of D_A also varies with sample position in this case, and a plot of eqn (S1) shows that all data points fall on a straight line; see **Fig. S5**. Accordingly, the fluctuating component of the scattering intensity, $\langle I_d \rangle_T$, denoted by the dashed lines in **Fig. S4**, and the collective diffusion coefficient, D, can be evaluated, as indicated in **Fig. S5**. The corresponding position dependence of $g^{(2)}(q,t) - 1$ is shown in **Fig. S6**. All the results reported in the main manuscript on the gel samples represent an average over 10–20 independent positions.

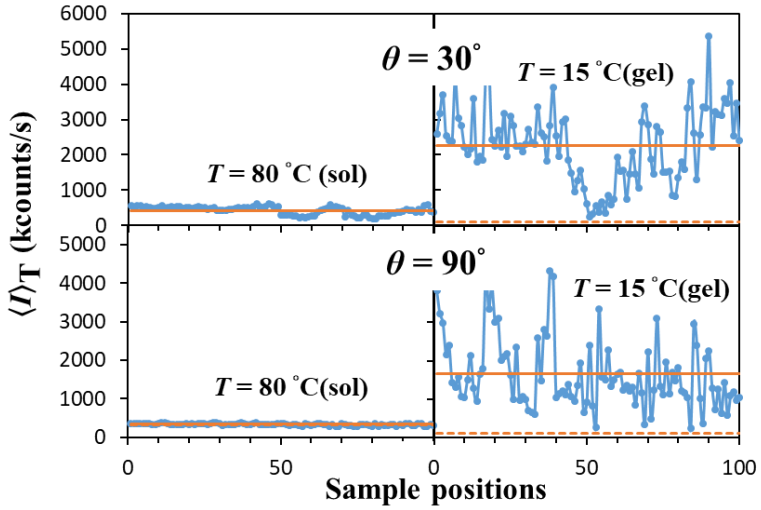

Fig. S4 Sample position dependences of time-averaged scattering intensity, $\langle I \rangle_T$, for Hw-pBTTT-C_{16}/CB solution (T = 80 °C) and gel (T = 15 °C; t = 24 h) at two representative scattering angles θ = 30° and 90°. The horizontal dashed and solid lines represent the results for $\langle I_d \rangle_T$ and $\langle I \rangle_E$, respectively.

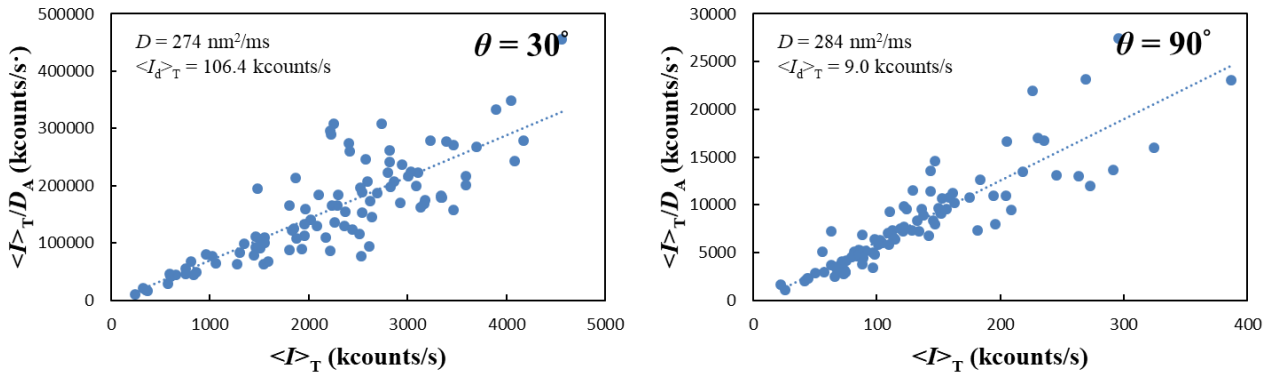

Fig. S5 Plots of $\langle I \rangle_T / D_A$ versus time-averaged scattering intensity, $\langle I \rangle_T$, for the Hw-pBTTT-C_{16}/CB gel incubated at 15 °C (t = 24 h), where the collective difussion coefficient, D, and the dynamic mobile component, $\langle I_d \rangle_T$, are obtained simultaneously by the slope and intercept, respectively, of the regressive line according to eqn (S1).

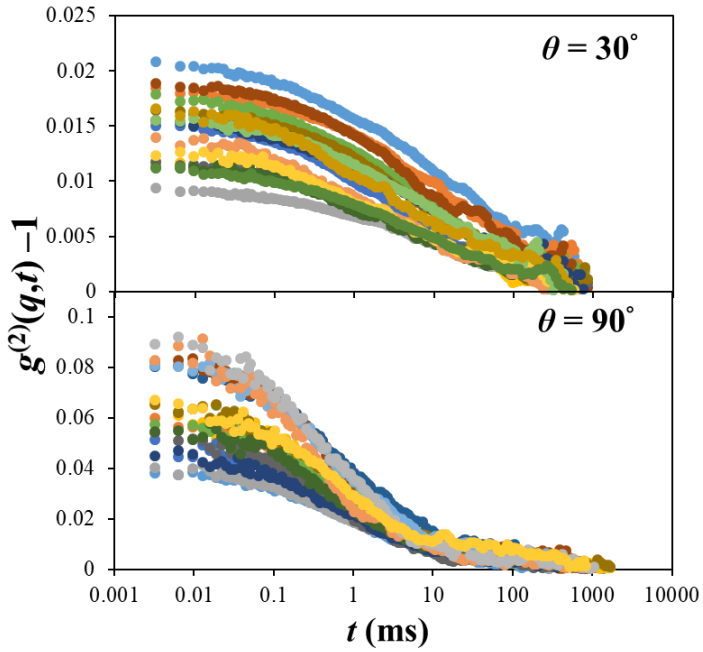

Fig. S6 Intensity correlation functions, $g^{(2)}(q,t) - 1$, measured at two representative scattering angles θ = 30° and 90° for different sample positions as considered in **Fig. S5** for the Hw-pBTTT-C_{16}/CB gel incubated at 15 °C (t = 24 h).

S5 Dynamic features of Hw-pBTTT-C_{16}/CB sol and gel

We first examine the time evolution of the normalized field autocorrelation functions, $|g^{(1)}(q, t)|$, shown in **Fig. 6a** of the main text, as the Hw-pBTTT-C_{16}/CB sol (t = 0 h) has been brought into the gel state at 15°C. As shown in **Fig. S7** for the initial (sol) state, $|g^{(1)}(q, t)|$ at various scattering angles do not collapse onto a single curve when the decay time is rescaled with q^2; this feature can also be seen in the CONTIN modes shown in the same figure, where three major modes may be identified (there is, in fact, a fourth mode at short times, possibly representing the sporadic gelators revealed in a later SAXS analysis). By taking into account the effect of some polydispersity in aggregate size, the scaling behaviors of the mean decay rate, $\langle\Gamma_i\rangle \sim q^{\alpha}$, shown in **Fig. 6b** of the main text suggest that the fast and intermediate modes are diffusive in nature, as the scaling exponents fall around 2. In contrast, the (third) slow mode is q-independent. The corresponding distributions of the mean hydrodynamic radius are presented in the inset of **Fig. 6a** in the main text, where the two (diffusive) aggregate species correspond to $R_h \sim 10$ nm and $R_h \sim 100$ nm (recall that the DDLS analysis indicated that the aggregate species for the initial (sol) state at 15°C is spherical in shape). As suggested by a later SAXS analysis, the fast mode represents the building particles of larger aggregate clusters, which in turn are manifested by the second (intermediate) mode.

The origin of the nearly q-independent relaxation ($\langle\Gamma\rangle \sim q^0$ in **Fig. 6b** of the main text) for the slow mode is of particular interest and worth pursuing. In general, similar relaxation behavior has been reported for a variety of polymer solutions,[19-24] where it customarily involved either elastic responses due to the formation of physical bonds, or chain relaxations subject to physical confinements (such as chain reptation). Interestingly, the analysis shown in **Fig. 6b** of the main text indicates that at an

intermediate stage of gelation (t = 8 h) the same slow mode has been transformed to a nearly q^2-dependent relaxation (*i.e.*, $\langle\Gamma\rangle = q^2$); meanwhile, we notice that the corresponding SAXS profile exhibits a notable increase in the fractal dimension (d_f = 2 to 3) in the low-q region, as shown in **Fig. S8**. These features together imply that the slow mode could represent certain *large yet loose* clusters, which begin to take shape as the gelation proceeds. At still longer times, these (micrometer-sized) clusters are among the first that interconnect to form the gel network, and the scaling law resumes to $\langle\Gamma\rangle \sim q^0$ again for a different reason, as seen in **Fig. 6b** of the main text for t = 16 and 24 h.

In **Fig. 6a** of the main text, the time-evolving $|g^{(1)}(q, t)|$ for the Hw-pBTTT-C_{16}/CB gel at 15 °C is observed to undergo the following stages: The initial (multiple-mode) exponential decay broadens substantially toward longer relaxation times, similar to the result of particle (or aggregate) clustering.[25] At intermediate times, the stretched exponential decay (at t = 8 h) transits to a power-law one (at t = 16 h). However, the long-time decay (at t = 24 h) appears to resume to an exponential type, a peculiar feature that had not been reported for polymer gels. Below, we perform detailed analyses of the DLS data to gain insight into these phenomena.

In the initial sol state (t = 0–8 h), three major relaxation modes have been identified in **Fig. 6b** of the main text. As discussed earlier, the fast mode may be attributed to the building particles of larger aggregate clusters (recall that these building particles represent the same rod-like species in the pristine solution at 80 °C that have since morphed into spherical ones at the gelation temperature). The second (intermediate) mode represents the diffusive (in sol) or collective (in gel) motion of the aggregate clusters, as described by the first term in eqn (S2) or (S3) discussed shortly. Described by the second term in the

same equation, the slow mode is associated with the translational diffusion of micrometer-sized clusters. With still longer gelation time (t = 16 h), the attributes of the first two modes change little while the third (slow) mode is indicative of arrested dynamics for micrometer-sized clusters. The overall power-law decay seen at this stage has previously been associated with the percolation threshold for polymers[26] as well as for irreversible aggregating silica,[27] copolymer micelles,[28] and thermoreversible (polymer-grafted) silica.[29] Finally (t = 24 h), a progressive drop in ICF (see **Fig. 5** in the main text) is known to be a signature of ergodic-to-nonergodic transition during gelation.[27,30-32] The wavy feature in the long-time relaxation of $|g^{(1)}(q, t)|$ has been suggested to be a consequence of low damping of acoustic waves that is typical in colloidal gels.[33] Detailed structural features are analyzed below.

For percolating systems, such as gelling polymer solutions[26] and colloid dispersions,[8,27,31,34] wherein individual chains or particles are being embedded in large aggregate clusters, the dynamic features have been well established both in theories and experiments. According to Martin and Wilcoxon,[35,36] the ICF in the sol state may be described by a fast mode (a single-exponential decay) and a slow mode (a stretched-exponential decay) as

$$g^{(2)}(q,t) - 1 = \sigma_I^2\{A \exp(-Dq^2t) + (1 - A) \exp[-(t/t_c)^\beta]\}^2 \quad \text{(S2)}$$

where σ_I^2 is the initial amplitude of ICF, A (≤1) is the fraction of the collective diffusion mode, D is the (collective) diffusion coefficient of the fast mode, t_c is the characteristic decay time for the stretched exponential mode, and β is the stretched exponent. The fits based on eqn (S2) for the DLS data (*i.e.*, $|g^{(1)}(q, t)|$) at t = 8 h are shown in **Fig. 6a** of the main text (solid lines).

When approaching a sol-gel transition point, the slow mode becomes dominant (when micrometer-

sized clusters in the present study interconnect to form the gel network), and the ICF becomes a power-law function which may be described by

$$g^{(2)}(q,t) - 1 = \sigma_I^2 \left\{ A \exp(-Dq^2 t) + (1 - A)\left[1 + \left(t/t^*\right)\right]^{(n-1)/2} \right\}^2 \quad \text{(S3)}$$

Here, t^* is the characteristic decay time when the power-law behavior emerges, and n ($0 < n < 1$) is the fractal dimension of the gel network.

It is important to note, however, that we here observe an initial stretched exponential decay of $|g^{(1)}(q, t)|$ followed by a plateau region at intermediate decay times for the Hw-pBTTT-C_{16}/CB gel at t = 24 h, indicative of restricted particle displacements and nonergodicity. A similar feature in $|g^{(1)}(q, t)|$ at long decay times has previously been attributed to the restructuring, aging, or re-equilibration event in weak colloidal gels.[29,37,38] In this case, the model proposed by Krall and Weitz[25] for the dynamics of fractal cluster gels may be utilized:

$$|g^{(1)}(q, t)| = \exp\left\{ -\frac{(q\delta)^2}{6}[1 - \exp(-t/\tau_\beta)^p] \right\} \exp(-t/\tau_\gamma)^{1.5} \quad \text{(S4)}$$

where δ^2 is the maximum mean-squared displacement of a segment of size q^{-1} (and, hence, may be used to infer the mean porosity size of a gel), τ_β is the characteristic decay time of density fluctuations, p is the argument of the stretched exponential decay, and τ_γ is the characteristic time for the aging behavior observed at long decay times. The exponential decay with a power exponent of 1.5 arises because of the local deformations by gel syneresis, which acts as force dipoles in the network.[38] The dotted lines in **Fig. 6a** of the main text (for t = 24 h) represent the best fits of $|g^{(1)}(q, t)|$ according to eqn (S4), where δ, τ_β, τ_γ, and p were usually treated as q-dependent parameters. It can be seen that the $|g^{(1)}(q, t)|$ curves at four different scattering angles can be described excellently by the fits with eqn (S4), and, notably, the

parameters are found to be independent of q.

Tracing back, a power-law fit with eqn (S3) is also carried out for t = 16 h (dashed lines) to determine the power-law exponent n, and its q^2 dependence is examined in **Fig. S9**. It appears that the values of n all fall around 0.54, in fair agreement with the "viscoelastic" exponents previously obtained by Michon et al. (*i.e.*, 0.6-0.71, depending on the polymer concentration and system temperature)[39] and by Okamoto et al. (*i.e.*, 0.74).[6] Thus, the q independence of n has been confirmed in the present study as well as in early work,[6,7] although the results reported by Ren et al. seem to exhibit a different trend.[40,41] Given that the exponent is physically related to the so-called viscoelastic exponent discussed earlier by Doi and Onuki,[42] the q independence seems to be more reasonable.

The power-law exponent, n, so determined may be used to estimate the fractal dimension d_f of the gel network. Models of this kind have been proposed for percolating polymers, varying mainly in their assumptions about hydrodynamic and excluded-volume interactions. There is a permitted range of n values for ensuring realistic fractal dimensions between 1 and 3. As the Rouse dynamics is assumed,[43] one has

$$n = \frac{3}{d_f+2} \tag{S5}$$

which requires the power-law exponent to fall in the range of $0.6 < n < 1$. If excluded-volume interactions are fully screened (yet with hydrodynamic interactions), d_f may be determined by[44]

$$n = \frac{3(5-2d_f)}{2(5-d_f)} \tag{S6}$$

with $0 < n < 1$ instead. Fractal dimensions estimated using the presently obtained power-law exponents along with eqn (S5) and (S6) are provided in **Table S1**, wherein it is evident that eqn (S6) better describes

the present data. Using the values of D previously obtained, the correlation length, ξ—a spatial length scale for describing the mean cluster separation (for sols) or mesh size (for gels)—can be estimated via the relation[45]

$$\xi = \frac{k_B T}{6\pi\eta D} \tag{S7}$$

The reduction of ξ (see **Table S1**) with increased gelation time is in accord with the progressive formation of a gel.

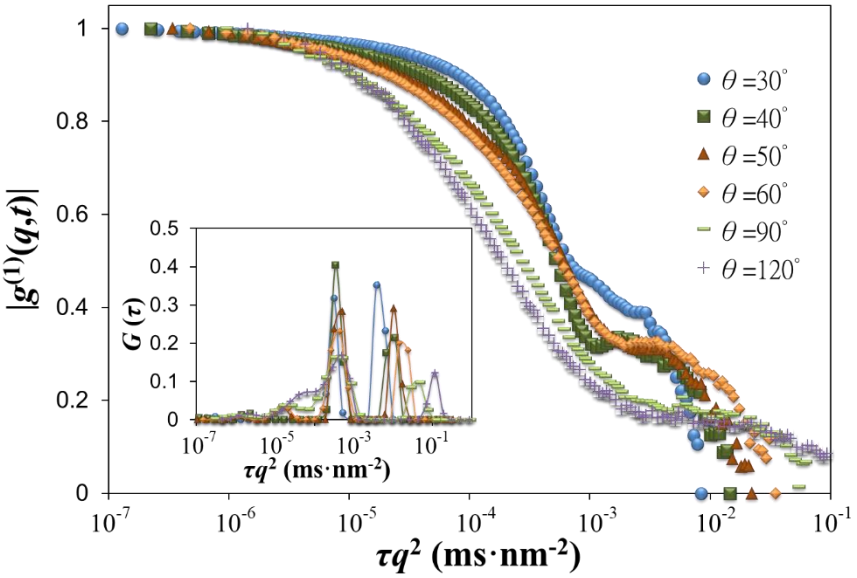

Fig. S7 Angular dependences of the field autocorrelation function, $|g^{(1)}(q, t)|$, for the Hw-pBTTT-C_{16}/CB gel incubated at 15 °C (t = 0 h), where the decay time τ has been rescaled with q^2. The corresponding decay time distribution functions, $G(\tau)$, extracted from CONTIN are shown in the inset figure.

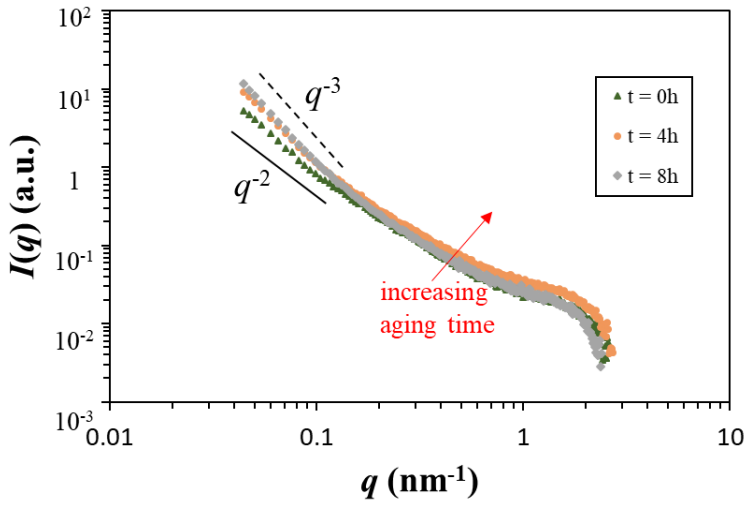

Fig. S8 Time evolutions of the SAXS profile for the Hw-pBTTT-C_{16}/CB gel at 15 °C, where symbols represent the results at three different gelation times: t = 0 h (green up-triangles), 4 h (orange spheres), and 8 h (gray diamonds), respectively.

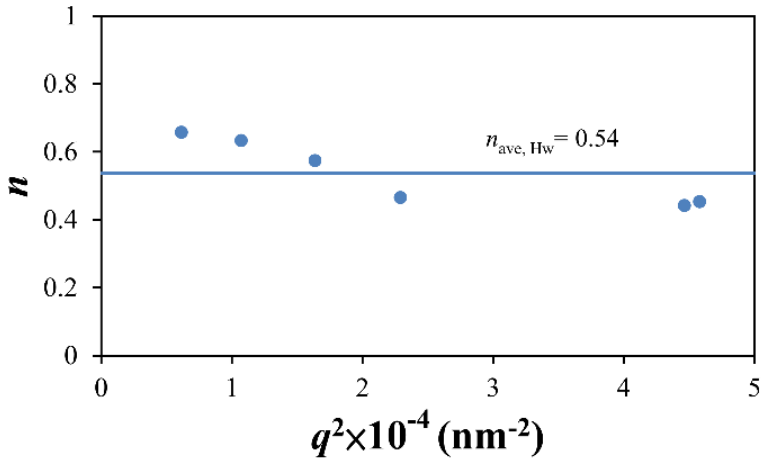

Fig. S9 q^2-dependences of the power-law exponent, n, determined from the fits to eqn (S3) using the data shown in **Fig. 6a** of the main text (dashed lines) for t = 16 h.

Table S1 Material properties extracted from DLS analysis for the Hw-pBTTT-C_{16}/CB sol and gel incubated at 15 °C

Methods	Parameters	Sol	Gel
DLS	Fraction of the collective diffusion mode (A)	0.78±0.09	0.10±0.07
	Collective diffusion coefficient (D) [$nm^2 \cdot ms^{-1}$]	107±21	283±67
	Characteristic time (t_c, t^*) [ms]	2.5±1.8	0.34±0.06
	Stretched exponent (β)/Power-law exponent (n)	0.95±0.12	0.54±0.11
	Fractal dimension (d_f)		
	-Rouse dynamics [a]	-	3.56
	-Hydrodynamic interactions [b]	-	1.95
	Correlation length (ξ) [nm] [c]	2334±458	883±209
	Maximum mean displacement (δ) [nm]	-	237±28
	Characteristic decay time of density fluctuations (τ_β) [ms]	-	0.31±0.17
	Stretched exponential decay (p)	-	0.25±0.08
	Characteristic time (τ_γ) [ms]	-	902±291

[a] Calculated from eqn (S5); [b] Calculated from eqn (S6); [c] Calculated from eqn (S7).

S6 Experssions used for the fitting of SALS/SLS/SAXS data

$$I(q) = I_{\mathrm{G}}(0)\exp\left(-\frac{1}{3}R_{\mathrm{g}}^2 q^2\right) + \frac{I_{\mathrm{L}}(0)}{\{1+[(d_{\mathrm{f}}+1)/3]\zeta^2 q^2\}^{d_{\mathrm{f}}/2}} P_{\mathrm{sph}}(q) \quad \text{(S8)}$$

where a spherical form factor is utilized (R being the radius):

$$P_{\mathrm{sph}}(q) = \left(3\,\frac{\sin(qR) - qR\cos(qR)}{(qR)^3}\right)^2 \quad \text{(S9)}$$

$$I(q) = \frac{I_{\mathrm{L}}(0)}{\{1+[(d_{\mathrm{f}}+1)/3]\zeta^2 q^2\}^{d_{\mathrm{f}}/2}} P_{\mathrm{sph,\ gelator}}(q) + I_{\mathrm{p}}(0) P_{\mathrm{sph,\ gelator}}(q) \quad \text{(S10)}$$

S7 Viscoelastic characterizations of Hw-pBTTT-C_{16}/CB solution and gels

Viscoelastic properties of Hw-pBTTT-C_{16}/CB solution and gels were characterized using three different rheological modes: (1) strain sweep with an angular frequency of 10.0 rad/s was used to identify the linear viscoelastic (LVE) region, as the sample solution was converted to the gel state at the gelation temperature (5, 10, and 15 °C); (2) frequency sweep was subsequently conducted with a (linear) strain amplitude of 0.01 to explore the variations of storage modulus (G') and loss modulus (G'') from solution to gel state (or the reverse process); (3) finally, the aging-time dependent, time-sweep complex modulus (G^*) data of Hw-pBTTT-C_{16}/CB gels were obtained using a strain amplitude of 0.01 along with a constant frequency of 10.0 rad/s.

We first perform (oscillatory) strain-sweep measurements to locate the linear viscoelastic (LVE) region of the Hw-pBTTT-C_{16}/CB gels investigated herein at a constant frequency of 10.0 rad/s. The results are shown in **Fig. S10**, with the central findings summarized as follows: All gels incubated at three different temperatures show constant magnitudes and solid-like behavior, $G' > G''$, at low strains. As the imposed strain exceeding a certain value in each case, the LVE region terminates and G' and G'' start to drop with increased strain magnitude. Near the crossover point of G' and G'', however, the Hw-pBTTT-C_{16}/CB gel exhibits a slight overshoot in G'' before it drops significantly with increased strain owing to the destruction of gel structure. Similar behavior, classified as a ‘‘weak strain overshoot,’’ was previously reported for a 4% xanthan gum solution[46] in strain-sweep experiment as well as in stress sweeps of mucin gels with properties similar to those of polyelectrolytes.[47,48] Comparatively, reducing the gelation temperature leads to a notable shortening of the LVE region, along with higher mechanical strength with

larger G' and G'' values.

In frequency-sweep measurements, a constant shear strain of 0.01 within the LVE range for all three samples is utilized to ensure that the gel properties are preserved without altering its microstructure. Moreover, the oscillatory frequency falls in a range of 0.01 to 300 rad/s to minimize the impact of fixture inertia. Results for a representative gelation temperature, T = 15 °C, are shown in **Fig. 9** of the main text for various stages of gelation (t = 0, 8, and 16 h), while the results on all three gel samples for t = 24 h are compared in **Fig. S11**.

To resolve the gelation kinetics, the following model derived by Li and Liu[49] for the Avrami theory of phase changes is employed:

$$\ln\left[-\ln\left(1-\phi_{\mathrm{g}}^{\mathrm{t}}\right)\right] = d_{\mathrm{f}}\left[\ln k + \ln\left(t - t_{\mathrm{gel}}\right)\right] \tag{S11}$$

where d_{f} is the Avrami component that reflects the fractal dimension of the gel structure, k is a rate constant proportional to the rate of gel growth, and t and t_{gel} are the elapsed time and the initial gelation time (*i.e.*, at $G' = G''$), respectively. The extent of gelation, $\phi_{\mathrm{g}}^{\mathrm{t}}$, (*i.e.*, how far the gelation proceeds from the initial sol state) can be expressed in terms of G^* at different times as $\phi_{\mathrm{g}}^{\mathrm{t}} = \left(G^*(t) - G_{\mathrm{bkg}}^*\right)/\left(G_{\mathrm{max}}^* - G_{\mathrm{bkg}}^*\right)$, where $G^*(t)$ is the time-dependent complex modulus, G_{bkg}^* is the complex modulus at the initial gelation time, and G_{max}^* is the maximum complex modulus at a kinetic equilibrium. Here, G_{max}^* is taken from the mean value of the modulus data at long times. Similar schemes have been used in early work to study the effects of solvent quality on the self-assembly behavior of PFO,[50] P3HT,[51] and MEH-PPV[52] organogels. For instance, $d_{\mathrm{f}} = 1$ indicates that the gel network is formed by following a 1-D kinetic pathway (*e.g.*, straight fibers); values between 1 and 2 imply bifurcated

or branching fiber growth; values between 2 and 3 correspond to spherulitic or sheet-like structures, and $d_f = 3$ indicates that the system is growing at an equivalent rate in all directions.

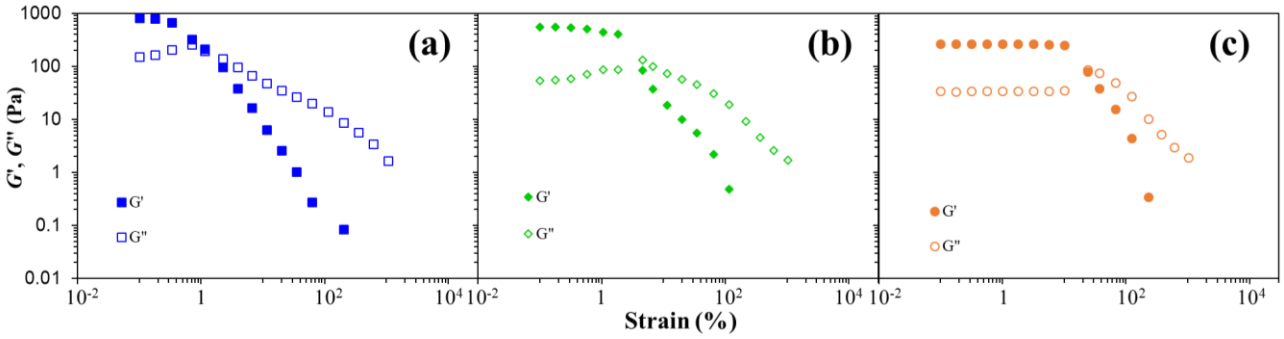

Fig. S10 Storage modulus G' (solid symbols) and loss modulus G'' (open symbols) obtained in strain-sweep measurements of the Hw-pBTTT-C_{16}/CB gels incubated at three different temperatures (t = 24 h): (a) 5 (squares), (b) 10 (diamonds), and (c) 15 °C (circles). Accordingly, a strain magnitude of 0.01 in the LVE region was used for the subsequent frequency-sweep measurements.

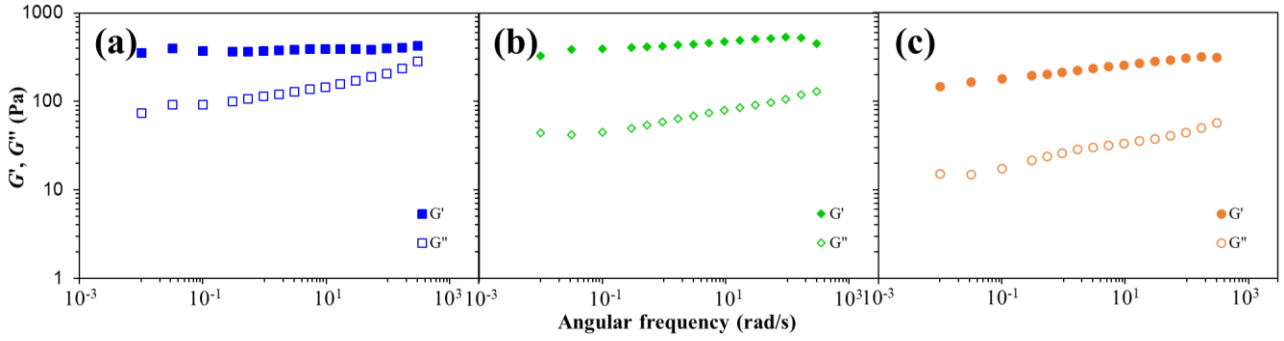

Fig. S11 Storage modulus G' (solid symbols) and loss modulus G'' (open symbols) obtained in frequency-sweep measurements of the Hw-pBTTT-C_{16}/CB gels incubated at three different temperatures (t = 24 h): (a) 5 (squares), (b) 10 (diamonds), and (c) 15 °C (circles).

References

1. P. N. Pusey and W. van Megen, *Phys. Rev. Lett.*, 1987, **59**, 2083-2086.
2. W. van Megen and P. N. Pusey, *Phys. Rev. A*, 1991, **43**, 5429-5441.
3. S. Mallam, A. M. Hecht, E. Geissler and P. Pruvost, *J. Chem. Phys.*, 1989, **91**, 6447-6454.
4. P. N. Pusey and W. Van Megen, *Phys. A*, 1989, **157**, 705-741.
5. F. Ikkai and M. Shibayama, *Phys. Rev. Lett.*, 1999, **82**, 4946-4949.
6. M. Okamoto, T. Norisuye and M. Shibayama, *Macromolecules*, 2001, **34**, 8496-8502.
7. M. Shibayama and M. Okamoto, *J. Chem. Phys.*, 2001, **115**, 4285-4291.
8. Y. Zhao, G. Zhang and C. Wu, *Macromolecules*, 2001, **34**, 7804-7808.
9. J. G. H. Joosten, E. T. F. Geladé and P. N. Pusey, *Phys. Rev. A*, 1990, **42**, 2161-2175.
10. J. G. H. Joosten, J. L. McCarthy and P. N. Pusey, *Macromolecules*, 1991, **24**, 6690-6699.
11. L. Fang and W. Brown, *Macromolecules*, 1992, **25**, 6897-6903.
12. C. Rouf, J. Bastide, J. M. Pujol, F. Schosseler and J. P. Munch, *Phys. Rev. Lett.*, 1994, **73**, 830-833.
13. B. J. Berne and R. Pecora, *Dynamic Light Scattering: With Applications to Chemistry, Biology, and Physics*, Dover Publications, New York, 2013.
14. M. Shibayama, T. Norisuye and S. Nomura, *Macromolecules*, 1996, **29**, 8746-8750.
15. M. Shibayama, Y. Fujikawa and S. Nomura, *Macromolecules*, 1996, **29**, 6535-6540.
16. M. Shibayama, S. Takata and T. Norisuye, *Phys. A*, 1998, **249**, 245-252.
17. M. Shibayama, *Macromol. Chem. Phys.*, 1998, **199**, 1-30.
18. T. Ngai, C. Wu and Y. Chen, *J. Phys. Chem. B*, 2004, **108**, 5532-5540.
19. M. Doi and S. F. Edwards, *The Theory of Polymer Dynamics*, Clarendon Press, New York, 1988.
20. K. Thuresson, S. Nilsson, A.-L. Kjøniksen, H. Walderhaug, B. Lindman and B. Nyström, *J. Phys. Chem. B*, 1999, **103**, 1425-1436.
21. A. Koike, N. Nemoto, T. Inoue and K. Osaki, *Macromolecules*, 1995, **28**, 2339-2344.
22. R. Johannsson, C. Chassenieux, D. Durand, T. Nicolai, P. Vanhoorne and R. Jerome, *Macromolecules*, 1995, **28**, 8504-8510.
23. G. Fytas, H. G. Nothofer, U. Scherf, D. Vlassopoulos and G. Meier, *Macromolecules*, 2002, **35**, 481-488.
24. J. Li, W. Li, H. Huo, S. Luo and C. Wu, *Macromolecules*, 2008, **41**, 901-911.
25. A. H. Krall and D. A. Weitz, *Phys. Rev. Lett.*, 1998, **80**, 778-781.
26. M. Takeda, T. Norisuye and M. Shibayama, *Macromolecules*, 2000, **33**, 2909-2915.
27. S. L. Elliott, R. J. Butera, L. H. Hanus and N. J. Wagner, *Faraday Discuss.*, 2003, **123**, 369-383.
28. F. Mallamace, P. Gambadauro, N. Micali, P. Tartaglia, C. Liao and S. H. Chen, *Phys. Rev. Lett.*, 2000, **84**, 5431-5434.
29. M. J. Solomon and P. Varadan, *Phys. Rev. E*, 2001, **63**, 051402.
30. S. Mitsuhiro and N. Tomohisa, *Bull. Chem. Soc. Jpn.*, 2002, **75**, 641-659.
31. T. Norisuye, M. Inoue, M. Shibayama, R. Tamaki and Y. Chujo, *Macromolecules*, 2000, **33**, 900-

905.
32. H. Guo, S. Ramakrishnan, J. L. Harden and R. L. Leheny, *Phys. Rev. E*, 2010, **81**, 050401.
33. M. Sztucki, T. Narayanan, G. Belina, A. Moussaïd, F. Pignon and H. Hoekstra, *Phys. Rev. E*, 2006, **74**, 051504.
34. X. J. Cao, H. Z. Cummins and J. F. Morris, *Soft Matter*, 2010, **6**, 5425-5433.
35. J. E. Martin and J. P. Wilcoxon, *Phys. Rev. Lett.*, 1988, **61**, 373-376.
36. J. E. Martin, J. Wilcoxon and J. Odinek, *Phys. Rev. A*, 1991, **43**, 858-872.
37. A. Mohraz and M. J. Solomon, *J. Colloid Interface Sci.*, 2006, **300**, 155-162.
38. L. Cipelletti, S. Manley, R. C. Ball and D. A. Weitz, *Phys. Rev. Lett.*, 2000, **84**, 2275-2278.
39. C. Michon, G. Cuvelier and B. Launay, *Rheol. Acta*, 1993, **32**, 94-103.
40. S. Z. Ren and C. M. Sorensen, *Phys. Rev. Lett.*, 1993, **70**, 1727-1730.
41. S. Z. Ren, W. F. Shi, W. B. Zhang and C. M. Sorensen, *Phys. Rev. A*, 1992, **45**, 2416-2422.
42. M. Doi and A. Onuki, *J. Phys. II*, 1992, **2**, 1631-1656.
43. D. Adolf and J. E. Martin, *Macromolecules*, 1990, **23**, 3700-3704.
44. W. Hess, T. A. Vilgis and H. H. Winter, *Macromolecules*, 1988, **21**, 2536-2542.
45. P. G. de Gennes, *Scaling Concepts in Polymer Physics*, Cornell University Press, New York, 1979.
46. K. Hyun, S. H. Kim, K. H. Ahn and S. J. Lee, *J. Non-Newtonian Fluid Mech.*, 2002, **107**, 51-65.
47. C. Taylor, A. Allen, P. W. Dettmar and J. P. Pearson, *Biochim. Biophys. Acta, Gen. Subj.*, 2004, **1674**, 131-138.
48. J. P. Celli, B. S. Turner, N. H. Afdhal, R. H. Ewoldt, G. H. McKinley, R. Bansil and S. Erramilli, *Biomacromolecules*, 2007, **8**, 1580-1586.
49. J.-L. Li and X.-Y. Liu, *Adv. Funct. Mater.*, 2010, **20**, 3196-3216.
50. P. de la Iglesia and D. C. Pozzo, *Soft Matter*, 2013, **9**, 11214-11224.
51. G. M. Newbloom, K. M. Weigandt and D. C. Pozzo, *Macromolecules*, 2012, **45**, 3452-3462.
52. R. H. Guo, C. H. Hsu, C. C. Hua and S. A. Chen, *J. Phys. Chem. B*, 2015, **119**, 3320-3331.